

Using DecaWave UWB Transceivers for High-accuracy Multipath-assisted Indoor Positioning

Josef Kulmer, Stefan Hinteregger, Bernhard Großwindhager, Michael Rath, Mustafa S. Bakr,

Erik Leitinger, Klaus Witrisal
Graz University of Technology, Austria
email: kulmer@tugraz.at

Abstract—Robust indoor positioning and location awareness at a sub-meter accuracy typically require highly accurate radio channel measurements to extract precise time-of-flight measurements. Emerging UWB transponders like the DecaWave DW1000 chip offer to estimate channel impulse responses with reasonably high bandwidth and excellent clock stability, yielding a ranging precision below 10 cm. The competitive pricing of these chips allows scientists and engineers for the first time to exploit the benefits of UWB for indoor positioning without the need for a massive investment into experimental equipment.

This work investigates the performance of the DW1000 chip concerning position related information that can be extracted from its channel impulse response measurements. We evaluate the signal-to-interference-plus-noise ratio of the line-of-sight and reflected multipath components which is a key parameter determining the Cramér-Rao lower bound on the ranging error variance. We propose a novel and highly efficient positioning algorithm, which requires information from a single anchor only. Results demonstrate reliable and robust positioning at an accuracy below 0.5 m.

I. INTRODUCTION

Location awareness is a key feature for many upcoming application scenarios, e.g. asset tracking, autonomous navigation or ambient assisted living [1]. This location awareness can be achieved outdoors via global navigation satellite systems (GNSS), e.g. GPS, Galileo, Beidou. For indoor environments, where GNSS fail due to low signal-to-noise-ratios (SNR) and multipath propagation, a reliable and robust, yet cost-effective alternative is still pursued.

Indoors, the radio-channel is heavily influenced by multipath propagation leading to severe fading and pulse dispersion. To reduce these effects, ultra-wideband (UWB) signals have been proposed due to their superior time-resolution [2]–[5]. This advantageous property of UWB transceivers comes at the expense of higher hardware costs compared to off-the-shelf radio transponders used in today's wireless sensor networks (e.g. Zigbee and Bluetooth Low Energy). However, with the emergence of UWB-chips like the DecaWave DW1000 [6] and the upcoming fifth generation (5G) of wireless networks, the cost for hardware components capable of providing high bandwidth signals is expected to fall over the next decade.

To further reduce hardware costs we propose to use single-anchor positioning techniques [1], [7], [8] which exploits

This work was performed in part within the LEAD-Project Dependable Internet of Things in Adverse Environments, funded by Graz University of Technology, and within the project REFlex, funded by the Austrian Research Promotion Agency (FFG; project number: 845630).

signal reflections by incorporating floorplan knowledge. These specular reflections at flat surfaces are modeled as deterministic multipath components (MPCs) which can be estimated from accurate channel measurements. Algorithms exploiting deterministic MPCs have been developed and evaluated using channel measurements performed with high-end equipment, e.g. vector network analyzers or correlative channel sounders. To avoid any synchronization errors, the transmitter and receiver antennas are both wired to the same measurement equipment. This allows to perform channel measurements even in challenging scenarios. Non-wired devices need to establish a connection and synchronize first. Once a connection is established, the clock accuracy has to be better than 1 ns to guarantee the required localization at sub-meter accuracy. These requirements are usually reflected in cost-intensive hardware.

The previously mentioned DecaWave DW1000 chip is an IEEE 802.15.4 (2011) compliant UWB transceiver which operates on 6 frequency bands with center frequencies between 3.5 to 6.5 GHz and a bandwidth of 500 or 900 MHz. It provides the possibility of range measurements and retrieving the measured channel impulse response (CIR) which is necessary to exploit deterministic MPCs. While the ranging capabilities of the DW1000 have been evaluated in [9], [10], the acquired CIR and the possible exploitation of MPCs have not been analyzed yet. We use the competitively priced Pozyx platform [11] which incorporates the DW1000 chip and a suitable UWB antenna.

The main contributions of this paper are:

- We analyze the range and CIR measurements of the Pozyx platform (see Section III),
- we evaluate the reliability of deterministic MPCs for ranging and positioning (Sec. III-E),
- and we derive a single-anchor approximate maximum likelihood position estimator (Sec. IV).

An implementation of the proposed positioning algorithm and the used data set are available to the research community at <http://www2.spse.tugraz.at/people/s0773094/dw>

II. PROBLEM FORMULATION

We are interested in individual channel measurements between two nodes, both located in an indoor environment. The anchor node is placed at known position $\mathbf{a} \in \mathbb{R}^2$ and the agent node at unknown position $\mathbf{p}_n \in \mathbb{R}^2$ with n as measurement index. The agent aims at localizing its position using radio

signals deteriorated by multipath propagation. The multipath propagation results from reflections of the radio signals with its surrounding environment. Knowledge of the environment enables to exploit rather than mitigate multipath propagation and allows to derive algorithms with improved accuracy and robustness.

A. Channel model

The channel impulse response of the propagation channel $h(t)$ is composed of deterministic and diffuse MPCs [4]

$$h(t) = \sum_{k \in \mathcal{K}} \alpha_k \delta(t - \tau_k) + \nu(t). \quad (1)$$

The first term on the right-hand-side models the deterministic MPCs $k \in \mathcal{K}$, each characterized by its complex-valued amplitude α_k and delay τ_k with $\delta(t)$ as Dirac delta function. These MPCs can be described using an environmental model, as further discussed in Section II-B. The second term of (1) is denoted as diffuse multipath (DM) $\nu(t)$. It models scattering, originating at small objects and rough surfaces. These scatters are not explained by the environmental model and therefore, they are treated as additive noise. We define the DM as zero-mean Gaussian random process with an auto-correlation function $\mathbb{E}_\nu \{ \nu(\tau)[\nu(u)]^* \} = S_\nu(\tau)\delta(\tau - u)$, introducing the uncorrelated scattering assumption [12]. Note, that the power delay profile $S_\nu(\tau)$ depends on both transmitter and receiver positions as well as the surrounding environment [13]. It is assumed to be stationary within a small region in the spatial domain (< 1 m) as discussed in III-E.

B. Relation to geometry

Deterministic MPCs describe specular reflections originating at flat surfaces, e.g. walls and windows. Assuming information of the surrounding environment to be available (e.g. a floorplan is provided), these reflections can be modeled using an *image-source model* [14], [15] as illustrated in Figure 1. The anchor's position \mathbf{a} is mirrored at each reflective surface to obtain *virtual anchors* (VA) \mathbf{a}_k , where each \mathbf{a}_k is assigned to a MPC k .

Then, the delay τ_k is the geometric distance between \mathbf{p}_n and \mathbf{a}_k , scaled by the propagation velocity c

$$\tau_k = \frac{1}{c} \|\mathbf{p}_n - \mathbf{a}_k\| \quad \text{for all } k \in \mathcal{K} \quad (2)$$

with $\|\cdot\|$ representing the Euclidean norm. Defining the physical anchor position by $\mathbf{a}_1 \triangleq \mathbf{a}$ and virtual anchors by $k > 1$, then the delays τ_k of the deterministic MPCs' can be calculated using Eq. (2).

The set of MPCs \mathcal{K} depends on the location of both communicating nodes. We verify the existence of potential MPCs using a ray-tracer [16, p. 34] where we do not consider effects like diffraction or diffuse scattering.

In general, deterministic MPCs are vital for the positioning algorithm as they provide position-related information. An open question is the model order of (1), in other words, which MPCs shall we include in \mathcal{K} . The obvious rule *the more the better* may easily result in a model bias. Considering

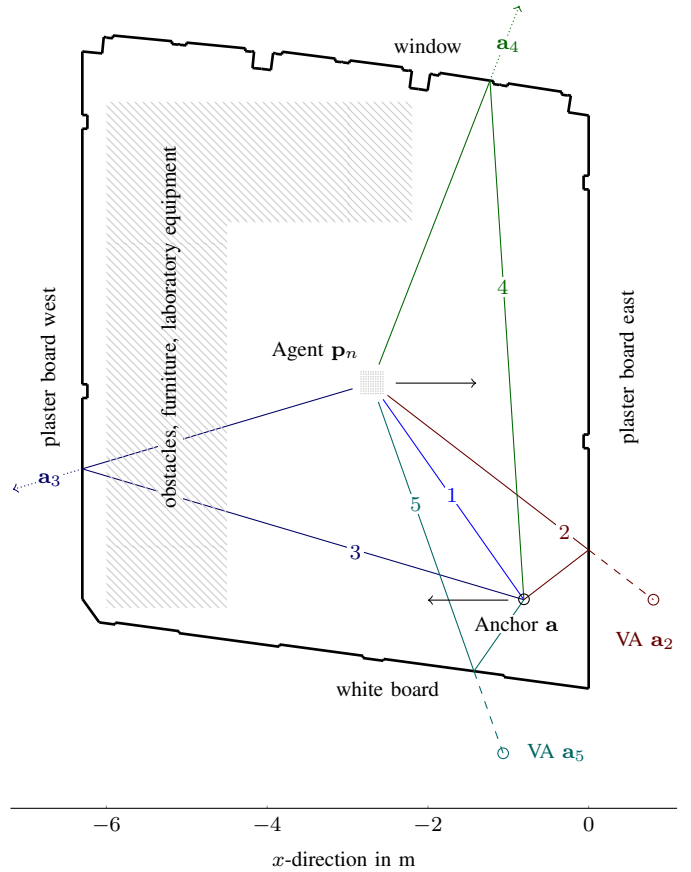


Fig. 1. Illustration of the floorplan and deterministic MPCs between an agent located at \mathbf{p}_n and anchor at \mathbf{a} . The line-of-sight ($k = 1$) and multipath propagation originating at plaster board east ($k = 2$) and west ($k = 3$), window ($k = 4$) and white board ($k = 5$) as well as their corresponding VA positions $\{\mathbf{a}_k\}_{k \in \mathcal{K}}$ are shown. The MPC at plaster board west is obstructed by furniture and laboratory equipment. The arrows next to agent and anchor indicate the orientation of the Pozzyx platform according to the coordinate system defined in [17, p. 15].



Fig. 2. Picture of the measured room. The anchor and agent positions as well as the surfaces generating the analyzed MPCs are labeled (cf. Fig. 1).

MPCs which are not contained in the impulse response (e.g. they are shadowed by other objects or strongly overlapped by DM) yield ambiguous results in the positioning algorithm. Therefore, we consider single-bounce reflections only as their visibility is more likely compared to MPCs which bounce several times before arrival. The importance of the MPC selection is further investigated in Sec. IV-B and IV-C.

C. Reliability of MPCs

We employ the signal-to-interference-plus-noise-ratio (SINR) [1] to describe the reliability of a specific MPC k . It relates the path energy $|\alpha_k|^2$ to the interfering DM, evaluated

at the MPC delay τ_k and scaled by the pulse duration T_p , and the measurement noise N_0 , according to

$$\text{SINR}_k = \frac{|\alpha_k|^2}{N_0 + T_p S_\nu(\tau_k)}. \quad (3)$$

The SINR has been demonstrated as reliability measure of MPCs suitable for the task of indoor positioning [4], [18]. In [1], [4] it was shown that the SINR endows a lower bound¹ on the squared error of the MPC delay estimation

$$\text{var}(\hat{\tau}_k) \geq (8\pi^2\beta^2\text{SINR}_k)^{-1} \quad (4)$$

with β as effective (root-mean-square) bandwidth.

III. ANALYSIS OF THE RECEIVED SIGNAL

This section presents an analysis of the capabilities of the low-cost experimental equipment and its potential to resolve and utilize multipath propagation. Subsection III-A introduces the hardware setup followed by presenting the reference system for comparison (III-B). In III-C and III-D device-specific parameters are discussed and in III-E results of the comparison between the low-cost equipment and the reference system are presented.

A. Measurement setup

Our work is based on the Pozyx platform which embeds the IEEE 802.15.4 (2011) compliant DecaWave DW1000 coherent UWB transceiver. Its dielectric chip antenna has an approximately uniform radiation pattern along its azimuth plane [17, p. 15].

The measurements were performed using two Pozyx nodes at positions \mathbf{a} and \mathbf{p}_n placed indoors under line-of-sight (LOS) conditions, 1.3 m off the floor, as illustrated in Figure 1. To take usage of the geometry model (Sec. II-B) we calculated the positions of the VAs by using a building floorplan where we considered flat surfaces with a minimum length of 25 cm. To ensure realistic conditions the room was furnished and equipped with several laboratory devices (see Figure 2). The furniture and equipment was not considered in the floorplan. We constrain the geometry model to two dimensions. The inevitable reflections at floor, ceiling, and furniture subsequently contribute to undesired, diffuse MPCs.

The DecaWave DW1000 is able to perform range measurements with an accuracy within ± 10 cm [6, p. 7]. Further, it allows to return the estimated CIR, sampled at $T_s = 1.0016$ ns with a length of 1016 samples (using a pulse repetition frequency of 64 MHz). It supports the UWB Channel numbers 2 – 5, standardized by IEEE 802.15.4 (2011). The Channels 2, 3 and 5 have a bandwidth of 0.499 GHz and Channel 4 1.331 GHz which is of particular interest due to its superior bandwidth.

To get insight into the impact of bandwidth on the estimated CIR, in the following, we analyze the Channels $C \in \{2, 4\}$, both located at center frequency $f_c = 3.994$ GHz. The measurements were performed with a pulse-repetition frequency of 64 MHz and 128 preamble symbol repetitions.

¹ Assuming the pulse shape $s(t)$ (introduced in Sec. III-D1) is known with a constant PSD and deterministic MPCs are assumed to be orthogonal $\int s(t-\tau_i)s(t-\tau_j)dt = 0$, for all $(\tau_i, \tau_j) \in \mathcal{K}, \tau_i \neq \tau_j$

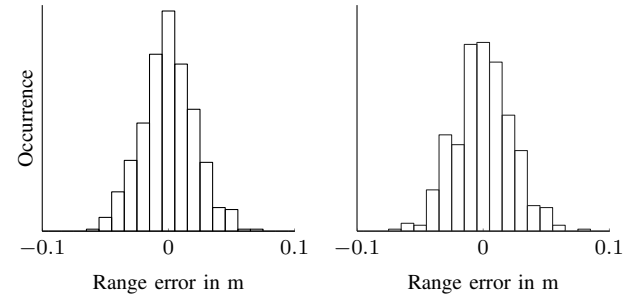


Fig. 3. Histogram of (calibrated) range error of Channel 2 (left) and Channel 4 (right).

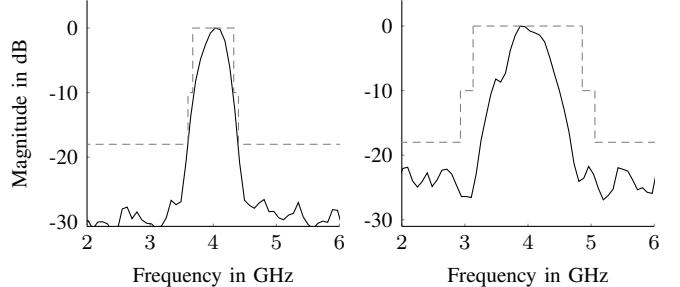


Fig. 4. Utilized radio-frequency band of DW1000 (black, solid) of Channel 2 (left) and Channel 4 (right) and the standardized transmit PSD mask (gray, dashed).

B. Reference system

As a reference we use CIR measurements obtained by an Ilmsens Correlative Channel Sounder (ICCS). It allows to measure the impulse response between two antennas, both wired to the ICCS. Calibration of the ICCS yields a negligible synchronization error. We used self-made Euro-cent coin antennas [19, p. 86] on both agent and anchor with approximately uniform radiation patterns in azimuth domain.

Due to measurement constraints of the ICCS, the carrier frequency was set to 4.34 GHz (which is slightly above DecaWave's $f_c = 3.994$ GHz, using Channels 2 and 4).

C. Range estimate

At each measurement Pozyx returns one measured range and the associated CIR. The measured range, denoted as d'_{DW} , is available in a resolution of 4.69 mm (which corresponds to one period of the 63.9 GHz ranging sampling clock [6, p. 8]). To calibrate the range estimates, we performed 1000 measurements of each channel and calculated the mean μ and standard deviation σ of the difference between the *true* distance of both Pozyx devices $\|\mathbf{p}_n - \mathbf{a}\|$ (measured with a tape) and the estimated ranges d'_{DW} . The resulting calibrated range estimates for each channel follow as $d_{\text{DW}} = d'_{\text{DW}} - \mu$. Figure 3 illustrates the histograms of the (calibrated) range errors of both channels. The observed standard deviations of Channel 2 (denoted as $\sigma_2 = 0.054$ m) and Channel 4 ($\sigma_4 = 0.053$ m) are comparable to the reported ones in [9], [10], [20].

We calculated the theoretical lower bound on the ranging precision (Eq. (4)) using the estimated SINR values in Ta-

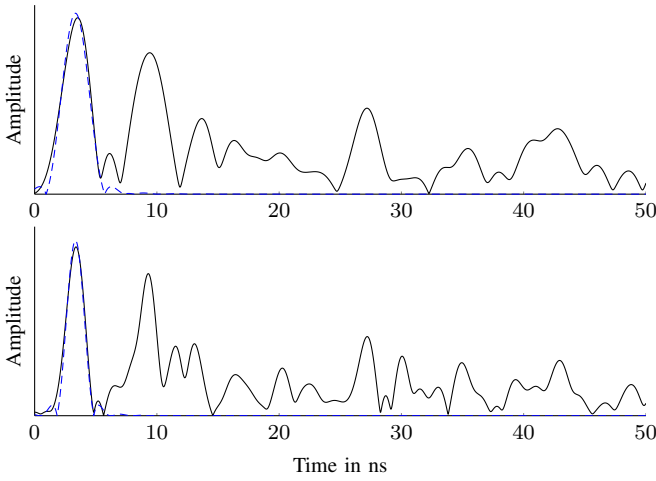


Fig. 5. Estimated channel impulse response (black, solid) of Channel 2 (top) and Channel 4 (bottom) and the approximated raised-cosine pulse (blue, dashed) shifted to the delay of the first path. For improved illustration the CIRs are interpolated by a sinc function.

ble I. The lower bound of the LOS $\text{var}(\hat{\tau}_1)$ is 0.029^2m^2 and 0.018^2m^2 for Channels 2 and 4, respectively. These values are below the ranging accuracy of the DW1000, which is presumably explained by the fact that Pozyx performs several measurements for the two-way ranging and for estimating the clock offset between the transceivers.

D. Channel impulse response

The measurement of a CIR is limited to physical constraints, e.g. limited bandwidth and clock errors. This section treats the DW1000 specifications in more detail and modifies the channel model in (1) accordingly.

To analyze the utilized spectral band, we used a real-time scope connected to a dipole-style UWB antenna [19, p. 86] via a high-performance low noise amplifier to assess the signal spectrum of the transmitted UWB signals. Time gating was used to isolate the LOS pulse. Figure 4 shows the power spectral density (PSD) (black, solid) in comparison with the transmit power spectral density mask (gray, dashed), specified in IEEE 802.15.4 (2011). Both channels comply with the standard. The under-utilization of Channel 4 is justified by DecaWave's limitation of Channel 4 to 900 MHz [6, p. 204]. The effective (root-mean square) bandwidth β of Channels 2 and 4 are $\beta_2 \approx 0.14 \text{ GHz}$ and $\beta_4 \approx 0.24 \text{ GHz}$.

Figure 5 exemplifies the estimated CIRs (black, solid) of Channel 4 (top) and Channel 2 (bottom) obtained from the DW1000. Both CIRs are composed of a separated LOS and several overlapping multipath components. The superior bandwidth of Channel 4 results in a higher time resolution, compared to Channel 2. Note, that the pulse shape is different at both channels, further, the CIR alignment along time domain includes an offset.

To address the impact of the observed pulse shape and CIR offset to the channel model, we describe the received signal by the DW1000 $r_{\text{DW}}(t)$ as a function of $h(t)$ according to

$$r_{\text{DW}}(t) = s(t) * h(t - t_0) + w(t) \quad (5)$$

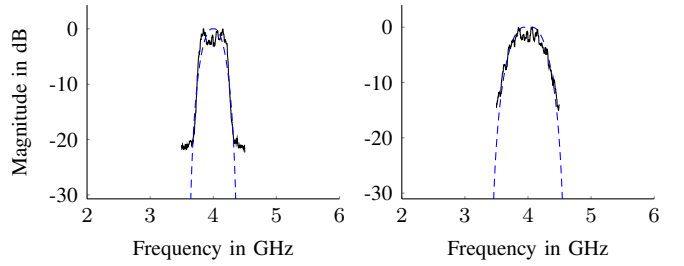


Fig. 6. PSD (black, solid) of Channel 2 (left) and Channel 4 (right) of DW1000's CIR. The PSD of the approximated pulse shapes (blue, dashed) is shown for comparison.

where $*$, $s(t)$ and t_0 denote the convolution operator, the (energy normalized) pulse shape and CIR offset, respectively, and $w(t)$ is additive white Gaussian noise.

1) *Pulse shape $s(t)$* : To get insight on the pulse shape, in the following, we disassemble the CIR to a convolution of transmitted signal $p_{\text{PHY}}(t)$, the channel impulse response $h(t)$ and a *UWB reference pulse*² $r_{\text{PHY}}(-t)$ and the pulse shape in (5) follows as $s(t) \triangleq p_{\text{PHY}}(t) * r_{\text{PHY}}(-t)$.

IEEE 802.15.4 (2011) standardizes $r_{\text{PHY}}(t)$ and a few requirements on the magnitude of $|p_{\text{PHY}}(t) * r_{\text{PHY}}(-t)|$. The transmitted signal $p_{\text{PHY}}(t)$ is not defined and depends on the actual implementation in the radio-frequency transmitter. Since the implementation is not published by DecaWave but required to estimate the path amplitudes using the proposed channel model in (5) we approximate $s(t)$ as a raised cosine pulse. The pulse parameters for Channel 2 (denoted as $s_2(t)$) are a pulse duration of $T_p = 2.4 \text{ ns}$ and roll-off factor of $R = 0.9$ and for Channel 4 ($s_4(t)$) we use $T_p = 1.5 \text{ ns}$ and $R = 0.8$. Figure 5 illustrates the approximated pulse shapes (blue, dashed), shifted to the location of the first path and Fig. 6 illustrates the PSD of DW1000's CIR (black, solid) in comparison with the pulse shape (blue, dashed).

2) *CIR offset t_0* : The Pozyx platforms do not share any absolute timing information of the stored CIR which results in an unknown t_0 in (5). We propose to employ the DW1000 range measurement d_{DW} to adjust the CIR offset. The range measurement is associated to the *leading edge* of the first path [6, p. 116]. Identification of the first path followed by shifting of the CIR enables the correct alignment.

To obtain the first path delay, we estimated the $N = 10$ strongest MPCs contained in each CIR using *search and subtract* [18], [22] and define the MPC with the lowest delay as first path. Subsequently, the CIR is shifted along time until the first path delay t_{first} matches with the ranging information d_{DW}/c , and the aligned CIR $r(t)$ follows accordingly from

$$r(t) = r_{\text{DW}}(t - t_{\text{first}} + d_{\text{DW}}/c). \quad (6)$$

It is important to note, that the ranging information obtained from the Pozyx platform may be erroneous which may result in a wrongly aligned CIR. The correct alignment is important to guarantee an accurate MPC parameter estimation and will be discussed in the following section.

² $p_{\text{PHY}}(t)$ and $r_{\text{PHY}}(t)$ are defined by the physical layer (PHY); IEEE 802.15.4 (2011) recommends a cross-correlation with $r_{\text{PHY}}(t)$ which is equivalent to a convolution with $r_{\text{PHY}}(-t)$

Table I: SINR in dB of deterministic MPCs for Channels 2 and 4 as well as both scenarios of CIR alignment with estimated (Scenario a) and expected ranges (Scenario b). The mean of the MPC's energy compared to the sum of all components, and SINR values obtained from Ilmsens Correlative Channel Sounder are shown for comparison. Low SINRs are subject to estimation errors [18], [21], indicated by *nan*.

MPC	Channel 2		Channel 4		$T_p = 2.4 \text{ ns}$	$T_p = 1.5 \text{ ns}$	Avg. distance	Energy
	a)	b)	a)	b)				
LOS	19.6	19.9	21.5	22.4	21.9	23.3	3.3 m	42 %
plaster board east	3.2	3.7	-2.7	-2.2	-0.2	4.6	4.4 m	7 %
plaster board west	-4.1	-2.3	<i>nan</i>	<i>nan</i>	-0.7	-2.7	9.5 m	2 %
white board	8.6	8.6	11.5	11.8	9.9	13.2	4.9 m	39 %
window	7.0	8.3	5.8	6.7	1.8	3.3	10.5 m	10 %

E. Analysis of MPCs for Ranging and Positioning

The previous sections offered potentials to embrace the DW1000's CIR. Finally, we will analyze the undertaken amendments in terms of SINR of selected MPCs. For this experiment, we placed one Pozyx at position \mathbf{a} where it remained for all measurements. The second Pozyx at \mathbf{p}_n moved on a 27×27 cm measurement grid with a spacing of 3 cm between adjacent measurement points, resulting in $n \in \{1, \dots, 100\}$ measurements, under LOS conditions (see Fig. 1).

We are interested in two scenarios: alignment of the CIR such that the first path delay t_{first} matches with

a) the Pozyx range estimate d_{DW}/c , equivalent to Eq. (6)

$$r_{\text{est}}(t) = r(t) \quad (7)$$

b) the expected first path delay, proportional to the actual distance between both platforms $\|\mathbf{p}_n - \mathbf{a}\|$

$$r_{\text{exp}}(t) = r_{\text{DW}}(t - t_{\text{first}} + \|\mathbf{p}_n - \mathbf{a}\|/c). \quad (8)$$

At both scenarios we employ the geometry model in (2) to predict the deterministic MPC delays $\{\tau_k\}_{k \in \mathcal{K}}$. We select those deterministic MPCs \mathcal{K} which exist at all measurement points, as illustrated in Figure 1. Then, for each MPC the amplitude results as projection of the received signal $r(t)$ onto the delayed pulse $s(t - \tau_k)$. Considering the Channels 2 and 4 the MPC amplitudes were estimated for all measurements n , using the appropriate signals $s_2(t)$ and $s_4(t)$, and both scenarios (Eq. (7) and (8)) of CIR alignment. Finally, the SINRs in (3) follow by employing a moment-based estimator [18] applied on the estimated amplitudes.

Table I reports the SINRs for the evaluated measurements and scenarios. The obtained SINRs using the reference system ICCS are shown for comparison. The measured impulse responses of the ICCS were shaped with the approximated pulse shapes $s_2(t)$ and $s_4(t)$ of Channel 2 and 4, respectively.

In general, it can be observed that the estimated SINRs of the Pozyx device are in a comparable range to the ICCS using a uniform radiation pattern. The LOS reaches the highest SINR whereas the deterministic MPCs at the window and the white board still reach SINR values, adequate to be used for localization. Both MPCs at plaster board walls achieve rather poor SINR values. This can be argued by the material's weak reflection properties as well as the laboratory equipment which is placed along the path of the MPC of plaster board west.

The SINR of the aligned CIR using Pozyx's range measurement (Scenario a) is slightly decreased, compared to the aligned CIR using the expected delay (Scenario b). This minor

degradation of 0 – 2 dB is caused by the uncertainty of the range measurement (see Fig. 3). The 3 dB main-lobe width of the auto-correlation function of $s_2(t)$ and $s_4(t)$ spans approximately (a time proportional distance of) 47 cm and 31 cm respectively. The range uncertainties σ_2 and σ_4 are much smaller than the 3 dB main-lobe width which explains the insensitivity of the SINR estimate with respect to the accuracy of the range estimate.

The estimated SINR levels are in a similar range to the ones reported in [18], which motivates exploitation of the MPCs for ranging and localization.

IV. LOCALIZATION USING POZYX

As shown in Table I the obtained CIR by DW1000 suffices to resolve and identify deterministic MPCs. In this section, we are interested if these MPCs can be further utilized. We focus on single-anchor localization [1], [7], [8] where an agent locates its position \mathbf{p}_n relying on time-of-arrival measurements to a single anchor at \mathbf{a} only. This application is of particular interest for low-cost solutions as the number of required anchor nodes can be reduced dramatically. We present an efficient algorithm for localization using the CIR and range measurements of the DW1000. Using the range estimate only with known \mathbf{a} , the position estimate of the agent $\hat{\mathbf{p}}_n$ is uniformly distributed on a circle around the anchor. The additional position-related information contained in the CIR [23] can be utilized to further identify the agent node's position.

A. Position estimation

In this section we derive an approximate maximum likelihood (ML) estimator for the agent position \mathbf{p} . Let \mathbf{r} denote the measured, complex-valued baseband CIR in vector notation, aligned according to (6) with a length of $T = 1016$. The pulse $s(t - \tau)$ shifted by delay τ , is denoted in vector notation as $\mathbf{s}(\tau) = [s(0 \cdot T_s - \tau), s(1 \cdot T_s - \tau), \dots, s((T-1) \cdot T_s - \tau)]^\top$ and the measurement noise follows as $\mathbf{w} = [w(0 \cdot T_s), w(1 \cdot T_s), \dots, w((T-1) \cdot T_s)]^\top$. Then, the signal model can be rewritten as

$$\begin{aligned} \mathbf{r} &= \sum_{k \in \mathcal{K}} \alpha_k \mathbf{s}(\tau_k) + \mathbf{w} \\ &= \mathbf{S}(\boldsymbol{\tau}) \boldsymbol{\alpha} + \mathbf{w} \end{aligned} \quad (9)$$

with $\boldsymbol{\tau} = [\tau_1, \dots, \tau_{|\mathcal{K}|}]^\top$, $\mathbf{S}(\boldsymbol{\tau}) = [\mathbf{s}(\tau_1), \dots, \mathbf{s}(\tau_{|\mathcal{K}|})]$, $\boldsymbol{\alpha} = [\alpha_1, \dots, \alpha_{|\mathcal{K}|}]^\top$ and $|\mathcal{K}|$ as number of deterministic MPCs.

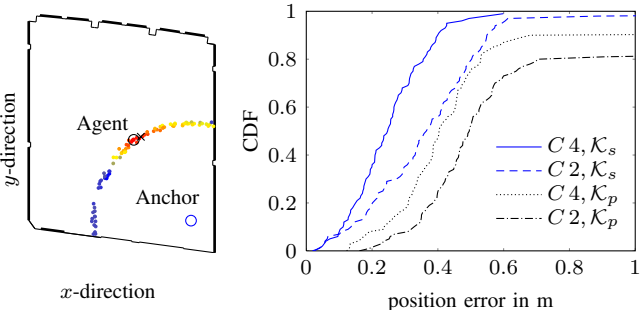


Fig. 7. Illustration of ML localization (left) utilizing multipath propagation. The agent is placed indoors (black cross) employing information of a single anchor (blue circle) to estimate its position (black circle). The CDF of 100 different positions (right) illustrates the impact of using deterministic MPCs predicted by the environmental model \mathcal{K}_p , and selected with reasonable high SINRs \mathcal{K}_s for both channels $C = \{2, 4\}$.

We simplify the channel model (1) by neglecting the DM and approximate the noise vector as a white, stationary Gaussian process³. The likelihood function of (9) with respect to the delays τ and amplitudes α then follows as

$$p(\mathbf{r}|\boldsymbol{\tau}, \boldsymbol{\alpha}) \propto \exp \left\{ -\|\mathbf{r} - \mathbf{S}(\boldsymbol{\tau})\boldsymbol{\alpha}\|^2 \right\}. \quad (10)$$

To simplify (10) we use the observation [24] that for a given $\boldsymbol{\tau}$ the amplitudes are calculated as linear least squares solution according to

$$\hat{\boldsymbol{\alpha}} = (\mathbf{S}(\boldsymbol{\tau})^H \mathbf{S}(\boldsymbol{\tau}))^{-1} \mathbf{S}(\boldsymbol{\tau})^H \mathbf{r}$$

with the superscript $(\cdot)^H$ as Hermitian transpose. To maximize (10) with respect to the agent position \mathbf{p} , the deterministic MPC delays $\boldsymbol{\tau}$ are substituted with \mathbf{p} and $\{\mathbf{a}_k\}_{k \in \mathcal{K}}$ using (2). Then the ML can be reformulated and the ML solution of the agent position estimate $\hat{\mathbf{p}}$ follows as

$$\hat{\mathbf{p}} = \underset{\mathbf{p} \in \mathcal{P}}{\operatorname{argmax}} p(\mathbf{r}|\mathbf{p}, \{\mathbf{a}_k\}_{k \in \mathcal{K}}). \quad (11)$$

A numerical evaluation of (11) is exhaustive since the ML function is multimodal and the set of possible solutions \mathcal{P} contains all positions within the communication range to the anchor [23]. We approximate (11) by considering I sampling points $\mathcal{P} = \{\mathbf{p}^{(i)}\}_{i=1}^I$. The sampling points are uniformly distributed around \mathbf{a} with a radius that is Gaussian with mean d_{DW} , i.e.

$$\begin{aligned} d^{(i)} &\sim \mathcal{N}(d_{DW}, \sigma^2) \\ \phi^{(i)} &\sim \mathcal{U}(0, 2\pi) \\ \mathbf{p}^{(i)} &= [d^{(i)} \cos(\phi^{(i)}), d^{(i)} \sin(\phi^{(i)})]^T + \mathbf{a} \end{aligned}$$

where $\mathcal{N}(\cdot, \cdot)$ and $\mathcal{U}(\cdot, \cdot)$ represent the Gaussian and Uniform distribution and σ^2 is the range variance from Sec. III-C. Sampling points which lie outside the area of interest (i.e. outside the room) are rejected.

³Note, that the discussed ML position estimator in [23] aims at finding an optimal solution (by employing SINR measurements) while in this work we introduce further approximations to obtain a practical solution

B. Evaluation using MPCs predicted by the environmental model

The following quantitative evaluation uses the environmental model to predict the set of deterministic MPCs \mathcal{K}_p , limited to first-order reflections (namely the MPCs in Table I)⁴. The agent was placed at $n \in \{101, \dots, 200\}$ positions \mathbf{p}_n on a 27×27 cm grid, different to the grid used in Sec. III-A. The anchor remained at the same position \mathbf{a} as in Sec. III-A.

The ML estimate in (11) (using \mathcal{K}_p) was applied to each n individually with $I = 100$ and the error between expected and estimated agent position follows as $\epsilon_n = \|\hat{\mathbf{p}}_n - \mathbf{p}_n\|$. Figure 7 exemplifies the floorplan (left) and the cumulative distribution function (CDF) of ϵ_n (right). The sampling points in \mathcal{P} are colorized according to the likelihood (10). A brighter color indicates that the underlying multipath propagation model fits better to the CIR observation. The maximum is marked with a black circle. We performed the evaluation for both channels 2 and 4. The resulting CDF of ϵ_n (Fig. 7 right) stimulates two interpretations. First, the superior bandwidth of channel 4 yields increased accuracy due to the improved possibility of MPC separation along time domain. Second, both CDFs barely reach the 90 % limit within 1 m. This can be reasonably argued as the algorithm expects deterministic MPCs at both plaster boards. Their rather low SINR values (see Table I) indicate that both MPCs are inadequate to be used for positioning. This finding can be interpreted as a biased channel model which subsequently results in a performance loss.

The following section evaluates the potential gain by selecting those MPCs with reasonable high SINRs.

C. Evaluation using selected MPCs

As reported in Table I, not all deterministic MPCs predicted by the environmental model are suitable to be exploited for localization. In this section we evaluate the derived ML estimator (11), limiting the deterministic MPCs to those with high SINRs, namely $\mathcal{K}_s = \{\text{LOS, window, white board}\}$. The agent and anchor positions as well as the parameters of the ML estimator were set similarly to Sec. IV-B. Figure 7 (right) compares the CDFs. We can observe that the position error of both channels is decreased and the 90 % limit is reached within approximately 0.5 m. The improvement may be counterintuitive since less deterministic MPCs are employed ($|\mathcal{K}_s| = 3$ compared to $|\mathcal{K}_p| = 5$). It is obtained because only those MPCs \mathcal{K}_s with high SINRs are used.

V. CONCLUSIONS

In this paper, we have evaluated the ranging and positioning capabilities of DecaWave's DW1000 incorporated into the Pozyx hardware platform. After analyzing the reliability of deterministic MPCs, we developed a positioning algorithm capable of using position related information contained in these MPCs using measurements to a single anchor only. The positioning error for a challenging indoor scenario is below

⁴The limitation to first-order reflections has been done for simplicity. Higher-order reflections have usually low SINRs (< 5 dB) at a bandwidth below 1 GHz [4]

0.5 m for both analyzed IEEE 802.15.4 (2011) channels. We can conclude that the Pozyx devices suffice to provide a CIR suitable for single-anchor localization. Selecting those deterministic MPCs that have high SINRs increases the performance. Our future work will expand the usage of low-cost hardware including tracking filters for synchronization and positioning.

REFERENCES

- [1] K. Witrisal, P. Meissner, E. Leitinger, Y. Shen, C. Gustafson, F. Tufveson, K. Haneda, D. Dardari, A. F. Molisch, A. Conti, and M. Z. Win, "High-accuracy localization for assisted living," *IEEE Signal Processing Magazine*, 2016.
- [2] D. Dardari, A. Conti, U. Ferner, A. Giorgetti, and M. Z. Win, "Ranging With Ultrawide Bandwidth Signals in Multipath Environments," *Proc. IEEE*, vol. 97, no. 2, pp. 404–426, 2009.
- [3] Y. Shen and M. Win, "Fundamental limits of wideband localization; part I: a general framework," *IEEE Transactions on Information Theory*, 2010.
- [4] E. Leitinger, P. Meissner, C. Ruedisser, G. Dumphart, and K. Witrisal, "Evaluation of position-related information in multipath components for indoor positioning," *IEEE Journal on Selected Areas in Communications*, 2015.
- [5] T. Nguyen, Y. Jeong, H. Shin, and M. Win, "Machine Learning for Wideband Localization," *Selected Areas in Communications, IEEE Journal on*, vol. PP, no. 99, pp. 1–1, 2015.
- [6] DecaWave, "DW1000 User Manual," Version 2.05, 2015.
- [7] R. Parhizkar, I. Dokmanic, and M. Vetterli, "Single-channel indoor microphone localization," in *2014 IEEE International Conference on Acoustics, Speech and Signal Processing (ICASSP)*, May 2014, pp. 1434–1438.
- [8] S. V. de Velde and H. Steendam, "CUPID algorithm for cooperative indoor multipath-aided localization," in *2012 International Conference on Indoor Positioning and Indoor Navigation (IPIN)*, Nov 2012, pp. 1–6.
- [9] J. Wang, A. K. Raja, and Z. Pang, "Prototyping and Experimental Comparison of IR-UWB Based High Precision Localization Technologies," in *IEEE Smart World Congress*, Aug 2015, pp. 1187–1192.
- [10] F. Hammer, R. Yudanto, K. Neumann, M. Pichler, J. Cockx, C. Niestroj, and F. Petré, "Performance Evaluation of 3D-Position Estimation Systems," *IEEE Sensors Journal*, vol. 16, no. 16, pp. 6416–6424, Aug 2016.
- [11] Pozyx - Accurate Positioning. [Online]. Available: <http://www.pozyx.io>
- [12] P. Bello, "Characterization of Randomly Time-Variant Linear Channels," *IEEE Transactions on Commun. Sys.*, vol. 11, no. 4, pp. 360–393, Dec 1963.
- [13] A. Molisch, "Ultra-wide-band propagation channels," *Proceedings of the IEEE*, 2009.
- [14] J. Borish, "Extension of the image model to arbitrary polyhedra," *The Journal of the Acoustical Society of America*, vol. 75, no. 6, pp. 1827–1836, 1984.
- [15] J. Kulmer, E. Leitinger, P. Meissner, S. Hinteregger, and K. Witrisal, "Cooperative localization and tracking using multipath channel information," in *2016 International Conference on Localization and GNSS (ICL-GNSS)*, June 2016.
- [16] P. Meissner, "Multipath-Assisted Indoor Positioning," Ph.D. dissertation, Graz University of Technology, 2014.
- [17] DecaWave, "DWM1000 Datasheet," Version 1.4, 2016.
- [18] P. Meissner and K. Witrisal, "Analysis of Position-Related Information in Measured UWB Indoor Channels," in *6th European Conference on Antennas and Propagation (EuCAP)*, 2012.
- [19] C. Krall, "Signal processing for ultra wideband transceivers," Ph.D. dissertation, Graz University of Technology, Austria, 2008.
- [20] W. Chantaweesomboon, C. Suwatthikul, S. Manatrinon, K. Athikulwongse, K. Kaemarungsi, R. Ranron, and P. Suksompong, "On performance study of UWB real time locating system," in *2016 7th International Conference of Information and Communication Technology for Embedded Systems (IC-ICTES)*, 2016, pp. 19–24.
- [21] L. J. Greenstein, D. G. Michelson, and V. Erceg, "Moment-method estimation of the Ricean K-factor," *IEEE Communications Letters*, vol. 3, no. 6, pp. 175–176, 1999.
- [22] C. Falsi, D. Dardari, L. Mucci, and M. Z. Win, "Time of arrival estimation for UWB localizers in realistic environments," *EURASIP Journal on Advances in Signal Processing*, vol. 2006, no. 1, pp. 1–13, 2006.
- [23] E. Leitinger, M. Froehle, P. Meissner, and K. Witrisal, "Multipath-Assisted Maximum-Likelihood Indoor Positioning using UWB Signals," in *IEEE ICC 2014 Workshop on Advances in Network Localization and Navigation (ANLN)*, 2014.
- [24] G. H. Golub and V. Pereyra, "The differentiation of pseudo-inverses and nonlinear least squares problems whose variables separate," *SIAM Journal on numerical analysis*, vol. 10, no. 2, pp. 413–432, 1973.